SJST
sjst.scst.edu.ly
Surman Journal for Science and Technology
ISSN: Online (2790-5721) - Print (2790-5713)
مجلة صرمان للعلوم والتقنية
Vol 6, No.2, Jun - Dec. 2024
Pages: 536 - 547

Estimation of Performance of the H Wind Turbine Using the Multiple Double Disk Stream Tube Theory

Mesbah. M. Salem[1], Ali Mohamed Elmabrok[2]
[1]The Libyan Academic, Sabha
[2]Faculty of Engineering, Tripoli university

Mesbahsalem1963@gmail.com[1], ali@aerodep.edu.ly[2]

Abstract

The performance of the H vertical axis turbine is comparable with that of the more common horizontal axis machines. It has a number of aerodynamic and structural advantages over HAWT'S. However, the H straight blade turbine is not self- starting at low wind speeds which is a considerable disadvantage for a simple small-scale installation. Generally, papers concerning vertical axis turbine do not study the behavior of the rotor at low tip speed ratios. Therefore, they do not deal with the self-starting problem.

A number of analytical methods were investigated to see whether they could predict the starting performance of vertical axis turbines. The Chosen methods used “actuator disc theory" for multiple Stream tubes. In this paper the multiple stream tube model is applied using two discs in tandem. The computational analysis of all models simulates the blade aerodynamics throughout the full range of incidence from -180° to 180°. The effects of varying various geometric parameters of the windmill upon the performance of the rotor are investigated to find a design with improved self-starting characteristics.

Key words: *Combined machine, Rotor, Windmill, blades, Vertical axis turbine*

INTRODUCTION

The vertical axis windmill generators are those machines which have their axis of rotation perpendicular to the wind direction. Vertical axis rotors have certain advantage over horizontal axis machines. Their operation is independent of wind direction; hence they don't have to yaw, or to turn when the wind changes direction, as they respond to wind from any direction. This advantage helps in reducing some of the complexity in design. Also, the vertical axis allows the torque to be transmitted directly to a generator on the ground, without the need for complicated gearing, thus engineering design is simplified and losses are reduced.

The H rotors are true lift type machines with airfoil shaped blades. Although the HAWT has been the most popular type of the wind turbine the vertical axis wind turbine (VAWT) is recognized as a machine with competitive economic potential.

Its configuration consists of two or three thin blades which have relatively low torque at low wind speeds but develop good power as the rotation speed increases.

The speed of rotation is primarily dependent on the machine's overall diameter. The interesting characteristic of this design is that the outer most parts of the blades revolve at three or four times the free stream velocity. The rotor configurations is shown in Fig. 1. In this paper the multiple double disk steam tube has been applied o model the performance and the self starting of the H wind turbine. In the stream tube models the induced velocity at the rotor is calculated by equating the time averaged force on the blades to the mean momentum flux

sjst.scst.edu.ly
Surman Journal for Science and Technology
ISSN: Online (2790-5721) - Print (2790-5713)
مجلة صرمان للعلوم والتقنية
Vol 6, No.2, Jun - Dec. 2024
Pages: 536 - 547

through a stream tube. The forces are calculated based on the local velocity and using the airfoil data concerning the lift and the drag coefficients, as a function of angle of attack and Reynolds number.

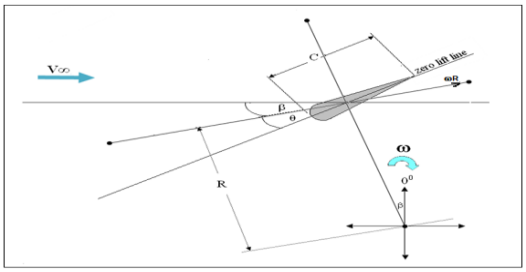

Fig 1: Blade element geometry

Aerodynamic Modeling

In the multiple stream tube theory as shown in Fig 2,

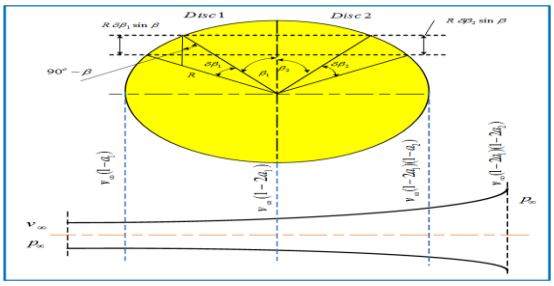

Fig 2 : stream tube geometry

a series of stream tube are assumed to pass through the rotor. In this model the induced axial velocity at the rotor is calculated by equating the time averaged force on the blade to the mean momentum flux through a stream tube of fixed location and dimensions. The forces are calculated based on the local velocity and the airfoil data concerning the lift and the drag coefficient, as a function of the angle of attack and Reynolds number.

The rate of change of momentum as the flow passes through the upstream disc and the downstream disc are as the following.

$$F_{xlm} = 2\rho\delta A_1 V_\infty^2 a_1(1-a_1) \qquad 1$$

$$F_{xlm} = 2\rho\delta A_2 V_\infty^2 a_1(1-a_1)^2(1-a_2)a_2 \qquad 2$$

The time averaged forces exerted on a blade in both upstream and downstream are given by the following equations.

$$\overline{F}_{x1b} = \frac{1}{2}\rho W_1^2 Cdy(C_{N1}\sin\beta - C_{T1}\cos\beta)N\frac{\Delta\beta}{2\pi} \qquad 3$$

$$\overline{F}_{x2b} = \frac{1}{2}\rho W_2^2 Cdy(C_{N2}\sin\beta - C_{T2}\cos\beta)N\frac{\Delta\beta}{2\pi} \qquad 4$$

Equating these equations to those given by the momentum theory yields

$$a_1 - a_1^2 = \left(\frac{W_1}{V_\infty}\right)^2 \frac{NC}{R}\frac{1}{8\pi} - (C_{N1}Sin\beta - C_{T1}Cos\beta) \qquad 5$$

sjst.scst.edu.ly
Surman Journal for Science and Technology
ISSN: Online (2790-5721) - Print (2790-5713)
مجلة صرمان للعلوم والتقنية
Vol 6, No.2, Jun - Dec. 2024
Pages: 536 - 547

$$a_2 - a_2^2 = \left(\frac{W_2}{V_\infty}\right)^2 \frac{NC}{R}\frac{1}{8\pi} - (C_{N2}Sin\beta - C_{T2}Cos\beta) \qquad 6$$

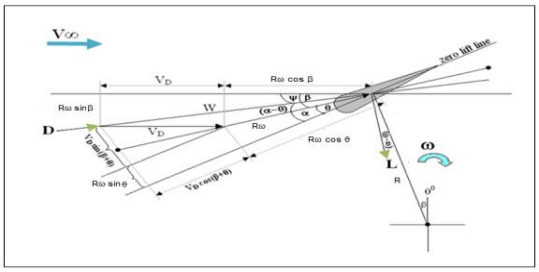

Fig 3: Blade element angles and velocities

The angle of attack and associated relative velocity in the plane of the air foil as shown in Fig 3 are obtained as follows

$$\alpha_1 = \arctan\left(\frac{(1-a_1)\sin\beta}{\lambda + (1-a_1)\cos\beta}\right) \qquad 7$$

$$\alpha 2 = \arctan\left(\frac{(1-2a_1)(1-a_2)\sin\beta}{\lambda + (1-2a_1)(1-a_2)\cos\beta}\right) \qquad 8$$

$$\left(\frac{W_1}{V_\infty}\right)^2 = (\lambda + (1-a_1)\cos\beta)^2 + ((1-a_1)\sin\beta)^2 \qquad 9$$

$$\left(\frac{W_2}{V_\infty}\right)^2 = (\lambda + (1-2a_1)(1-a_2)\cos\beta)^2 + ((1-2a_1)(1-a_2)\sin\beta)^2 \qquad 10$$

Torque and the Power of Darrieus Rotor

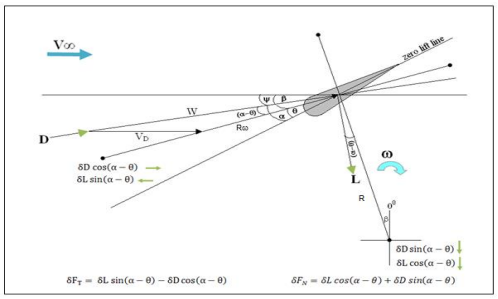

Fig 4: Blade tangential and normal forces

The upstream local thrust force and the downstream exerted by an individual blade element as shown in Fig 4, are given by the following equations

$$\delta F_{t1} = \frac{1}{2}\rho W_1^2 C dy C_{T1} N \frac{\delta\beta}{2\pi} \qquad 11$$

SJST
sjst.scst.edu.ly
Surman Journal for Science and Technology
ISSN: Online (2790-5721) - Print (2790-5713)
مجلة صرمان للعلوم والتقنية
Vol 6, No.2, Jun - Dec. 2024
Pages: 536 - 547

$$\delta F_{t2} = \frac{1}{2}\rho W_2^2 C dy C_{T2} N \frac{\delta\beta}{2\pi}$$

The torque coefficient of Darrieus machine is calculated using the multiple Stream tube model, which use a double disk model with the final expression of the torque is given as the following;

$$C_Q = \frac{3}{4}\frac{NC}{R}\frac{1}{2\pi}\left(\int_0^1\int\left[\left(\frac{W_1}{V_\infty}\right)^2 C_{T1}\ K_1 + \left(\frac{W_2}{V_\infty}\right)^2 C_{T2}\ K_2\right]\partial\beta\,\partial y \qquad 13$$

Were.

$$K_1 = \frac{(1-2a_1)(1-a_2)}{(1-a_1)+(1-2a_1)(1-a_2)}$$

$$K_2 = \frac{(1-a_1)}{(1-a_1)+(1-2a_1)(1-a_2)}$$

The above integral is evaluated over upwind azimuth angles and over downwind azimuth angles

And the following relation calculates the power coefficient;

$$C_P = \lambda\ C_Q \qquad 14$$

The procedures for carrying out computation on a specified stream tube to predict the rotor performance are as follows:

1- a_1 is set equal to zero at certain starting azimuth angle

2- α_1 is obtained from equation (7).

3- CN_1, C_{T1} are obtained from airfoil data.

4- $(W_1/V_\infty)^2$ is obtained from equation (9).

5- The new value of a_1 is computed using equation (5)

6- The process is repeated starting with calculation of α until the desired accuracy in a_1 is obtained.

7- Knowing the value of a_1, the value of a_2 could be calculated following the same procedures those are illustrated above to calculate the upstream inflow factor, and then both the local torque of the upstream half cycle and the local torque coefficient of the downstream half cycle corresponding to the azimuth angle and could be calculated.

8-Repeat the previous for a complete revolution, and along the rotor span (-H/2<Y<H/2).

9- Calculate the average torque coefficient and the average power coefficient by using Equation (15).

sjst.scst.edu.ly
Surman Journal for Science and Technology
ISSN: Online (2790-5721) - Print (2790-5713)
مجلة صرمان للعلوم والتقنية
Vol 6, No.2, Jun - Dec. 2024
Pages: 536 - 547

Results and Discussion

Variation of the blade angle of attack. Figures 5, 6,

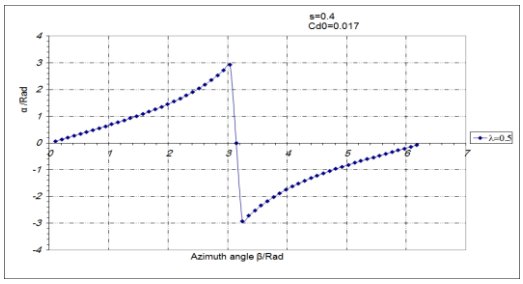

Fig 5: Variation of angle of attack α versus the azimuth Angle β at λ=0.5

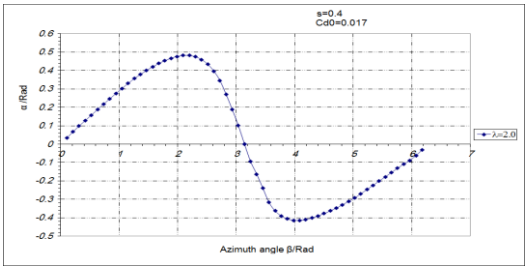

Fig 6: Variation of angle of attack α versus azimuth angle β at λ =2

indicate the variation of the angle of attack as a function of tip speed ratios. It is clear from these figures that the angle of attack is positive in the upwind half of the cycle ($0^o \leq \beta \leq 180^o$) and negative in the downwind half ($180^o \leq \beta \leq 360^o$). As can be seen from these figures, the value of the angle of attack increases as the azimuth angle increases until it reaches its maximum value then the angle of attack decreases as the azimuth angle increases. It is also noted that for a given value of azimuth angle, the value of the angle of attack increases as the tip speed ratio decreases (low tip speed ratio) this leads to an aerodynamic stall, which causes the low starting torque (self starting problem).

However as shown in Fig. 7,

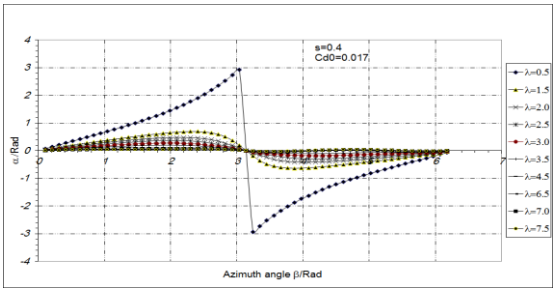

Fig 7: Variation of angle of attack α versus the azimuth Angle β for ($0.5 \leq \lambda \leq 7.5$)

for a fixed value of azimuth angle the angle of attack decreases as tip speed ratio increases and becomes very small at high values of tip speed ratio. this causes a negative thrust coefficient at higher values of tip speed ratio.

sjst.scst.edu.ly
Surman Journal for Science and Technology
ISSN: Online (2790-5721) - Print (2790-5713)
مجلة صرمان للعلوم والتقنية
Vol 6, No.2, Jun - Dec. 2024
Pages: 536 - 547

Rotor Torque Results.

The torque coefficient is directly dependent on many parameters such as the blade azimuth angle "β" and tip speed ratio "λ".

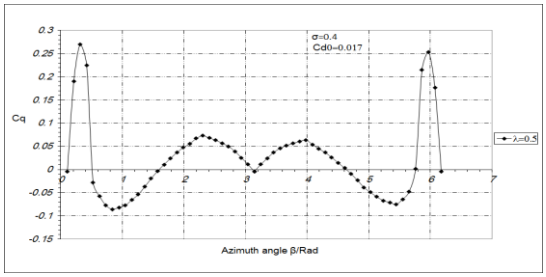

Fig 8: variation of local torque coefficient versus azimuth angle for (λ=0.5), (G=1, σ=0.4, C_{d0}=0.017)

Figure 8 presents C_q(β)curves for a constant value of σ=0.4, C_{d0}=0.017 and λ=0.5. It can be seen from this figure that the torque coefficient increases as the azimuth angle "β" increases until it reaches its maximum value (aerodynamic stall α=α_{stall}). Beyond stalling, the value of the torque coefficient "C_q" decreases as the azimuth angle increases till reaches its minimum value. Subsequently the torque coefficient increases and becomes positive. Due to the symmetry of the NACA-0018 section the "C_q-β" curves almost repeat themselves in reverse from (180ºto 360º), the small differences are due to the effect of downstream inflow factor .

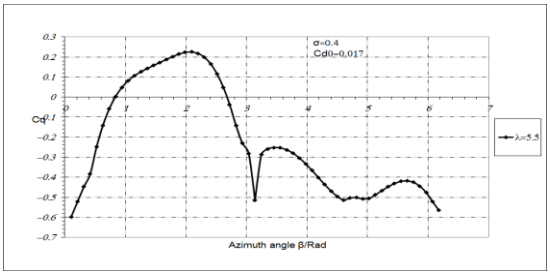

Fig 9: variation of local torque coefficient versus azimuth angle for (λ=5.5), (G=1, σ=0.4, C_{d0}=0.017)

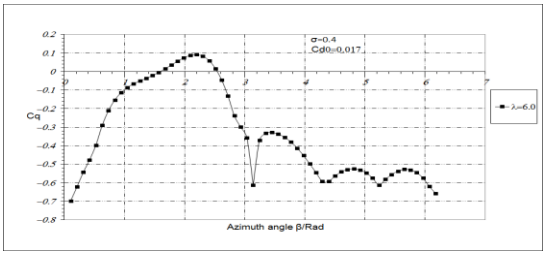

Fig 10: variation of local torque coefficient versus azimuth angle for (λ=6), (G=1, σ=0.4, C_{d0}=0.017)

Figs 9, 10 show that at higher values of tip speed ratio (λ=5.5, λ=6.0), the local torque coefficient is negative over most of values of the azimuth angle range this causes a negative value of torque coefficient and that due to lower values of the angle of attack at high values of tip speed ratios.

sjst.scst.edu.ly
Surman Journal for Science and Technology
ISSN: Online (2790-5721) - Print (2790-5713)
مجلة صرمان للعلوم والتقنية
Vol 6, No.2, Jun - Dec. 2024
Pages: 536 - 547

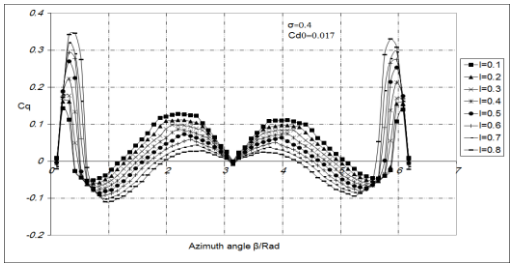

Fig 11: variation of local torque coefficient versus azimuth angle for $0.1 \leq \lambda \leq 0.8$, G=1, σ=.4, Cdo=0.017

Fig 11, indicates the variations of the local torque coefficient $C_q(\beta)$for a constant value of σ=0.4 and C_{d0}=0.017 over low λ-range ($0.1 \leq \lambda \leq 1$). This figure show that all curves show a similar behavior. This figure also shows that for a fixed value of azimuth angle (β) the maximum amplitude of the positive torque region increases as the value s of the tip ratios increases, while the minimum amplitude of the negative torque region decreases as the value of tip speed ratio increases. This differences rate of variations causes the decreasing of the average torque coefficient at low tip speed This due to variation of the angle of attack over this range of tip speed ratios.

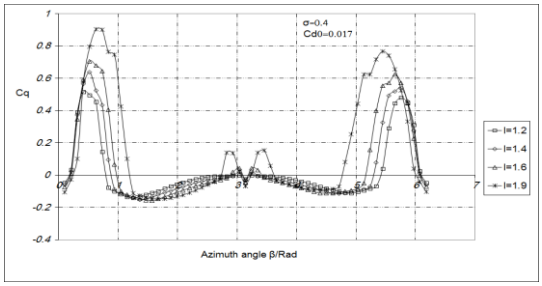

Fig 12: variation of local torque coefficient versus azimuth angle for ($1 \leq \lambda \leq 2$), (G=1, σ=0.4, C_{d0}=0.017)

Fig 12, shows a similar behavior as in fig 11, concerning the variation of azimuth angle and the local torque coefficient. The only difference between them is that over the range ($1 \leq \lambda \leq 2$) the average torque coefficient increases as the tip speed ratio increases due to variation of the angle of attack. This trend continues until ($\lambda = 3.5$).

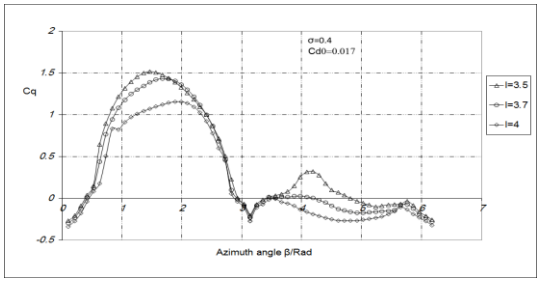

Fig 13: variation of local torque coefficient versus azimuth angle for ($3.5 \leq \lambda \leq 4$), (G=1, σ=0.4, C_{d0}=0.017)

sjst.scst.edu.ly
Surman Journal for Science and Technology
ISSN: Online (2790-5721) - Print (2790-5713)
مجلة صرمان للعلوم والتقنية
Vol 6, No.2, Jun - Dec. 2024
Pages: 536 - 547

Then for values of λ> 3.5, it is clear from figure 13, the local torque coefficient decreases as the tip speed ratio increases due to the effect of the angle of attack at higher values of tip speed ratios.

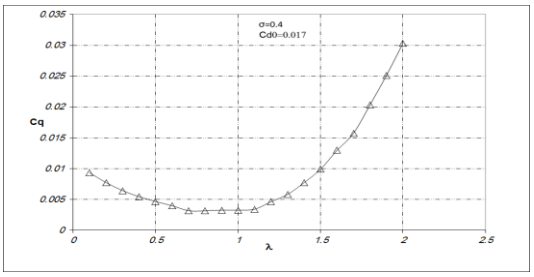

Fig 14: Rotor torque coefficient versus low value, tip speed ratio (G=1, σ=0.4, C_{d0}=0.017**)**

Fig 14, shows the variation of the model average torque C_q of the whole turbine versus tip speed ratio in the range ($0.1 \leq \lambda \leq 2$). It is clear that the average torque coefficient decreases as the tip speed ratio increases from (0.1 to 1.1) while for the range of tip speed ratio, ($1.1 \leq \lambda \leq 2$), the average torque coefficient increases as the tip speed ratio increases. This is due to the variation of the angle of attack in these regions.

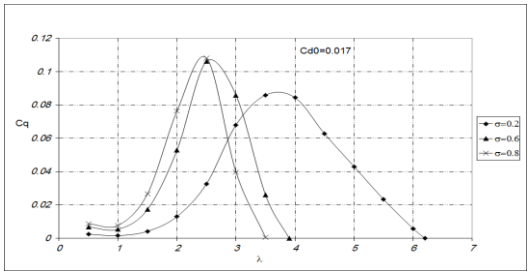

Fig 15: The effect of solidity on rotor torque coefficient for (G=1, $0.2 \leq \sigma \leq 0.8$, C_{d0}=0.017)

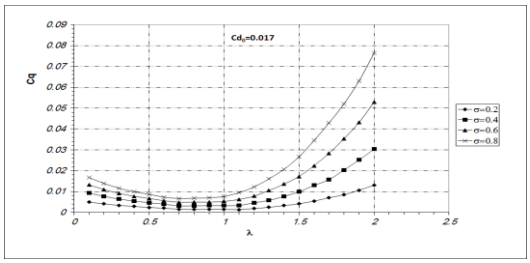

Fig 16: The effect of solidity on rotor torque coefficient for (G=1, $0.2 \leq \sigma \leq 0.8$, Cd0=0.017)

Figs 15 and 16, presents ($C_q(\lambda)$) curves at constant value of (C_{d0}) of 0.017 and constant value of (G) of 1.0, and values of (σ) equal to 0.2, 0.6 and 0.8. Fig 16, shows that the maximum value of the torque coefficient C_{qmax} increases as σ increases. It is noted that the value of λ at which C_{qmax} occurs shifts towards lower values as σ increases. Increasing the value of σ reduces the operating range of λ. It is also noted from these two figures that over low λ- range ($0.5 \leq \lambda \leq 2.5$) as σ increases the value of (C_q) increases, while C_q decreases as (σ) increases over high (λ) range ($2.5 \leq \lambda \leq 6.0$). This behavior is due to the variation of the angle of attack at low and high values of tip speed ratios. Thus, higher values of rotor solidity may help to improve the possibility of rotor self-starting.

sjst.scst.edu.ly
Surman Journal for Science and Technology
ISSN: Online (2790-5721) - Print (2790-5713)
مجلة صرمان للعلوم والتقنية
Vol 6, No.2, Jun - Dec. 2024
Pages: 536 - 547

Rotor power results.

The rotor power coefficient is dependent on many parameters such as rotor solidity, blade aerofoil zero-lift drag coefficient.

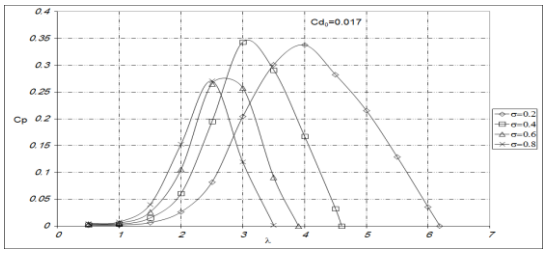

Fig 17: The effect of solidity on rotor power coefficient for (C_{d0}=0.017, 0.2 ≤ σ ≤ 0.8)

Fig 17, presents Cp (λ) for a constant value of C_{d0}=0.017and value G of 1.0 and values of σ equal to o.4, 0.6, 0.8. This figure indicates that the variation of the power coefficient as a function of the solidity is similar to that observed in case of the torque coefficient Fig 15. The only difference is that as σ increases the maximum value of power coefficient, C_{pmax} increases at first then it decreases.

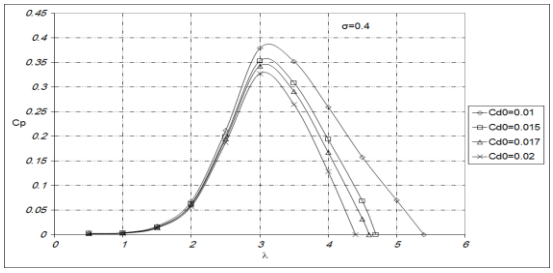

Fig 18: The effect of Zero lift drag coefficient on power coefficient (σ=0.4)

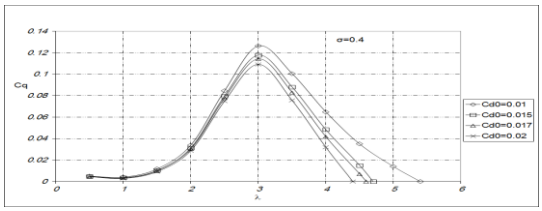

Fig 19 The effect of Zero lift drag coefficient on torque coefficient (σ=0.4)

Figures 18 and 19 indicate the effect varying the blade aerofoil zero-lift drag Coefficient on both the power coefficient and the torque coefficient respectively. Fig 18 indicates that at constant values of (σ=0.4) and (G=1.0), the power coefficient increases as the value of (C_{d0}) decreases over the whole range of λ. It is noted of that the maximum value of power coefficient (C_{pm}) increases as C_{d0} decreases, also it can be seen the decreasing the value of C_{d0} increases the operation range of λ. The relative increase of Cp with the decrease of C_{d0} is substantially higher over high λ-range, and that because over low range of tip speed ratios the angle of attack is very high which means that the profile drag is small fraction of the total drag coefficient, while over high λ-range the vice is versa.

sjst.scst.edu.ly
Surman Journal for Science and Technology
ISSN: Online (2790-5721) - Print (2790-5713)
مجلة صرمان للعلوم والتقنية
Vol 6, No.2, Jun - Dec. 2024
Pages: 536 - 547

Fig 19, shows ($C_q(\lambda)$) curves for a constant value of (σ) of 0.4. It is clear that the ($C_q(\lambda)$) curve have a similar behavior as (C_p/λ) in Fig18.

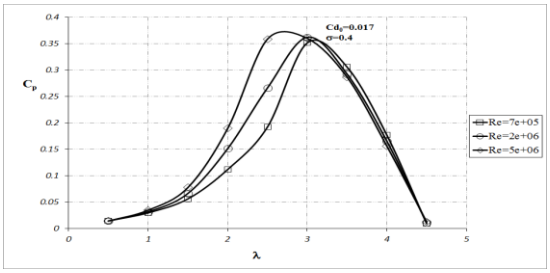

Fig .20: The effect of Reynolds number on power coefficient For (σ=0.4, C_{d0}=0.017)

Figure 20, indicates the effect of varying Reynolds number (Re) on the power coefficient (C_p) for three models having a fixed value of (σ) of 0.4 and (C_{d0}) of 0.017. It is clear that an increase in (Re) leads to an increase in (C_p) over the whole range of (λ) due to the delay of the blade stalling. It is also noted that the rate of increasing of (C_p) is very low over the low (λ) range ($0.5 \leq \lambda \leq 1.5$), compared with the range of ($1.5 < \lambda < 3$), this due to the variation of the angle of attack for both ranges.

Comparison of Theoretical and Experimental Results

In order to validate the results of this work, the results of this program were compared with other results obtained by other references.

The comparison of the theoretical results and the corresponding results obtained from ref [10], are shown in Figs 21, and 22.

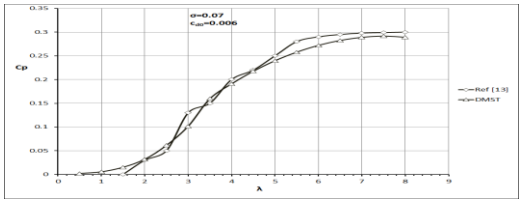

Fig 21: comparison of theoretical results C_p with ref[10] results

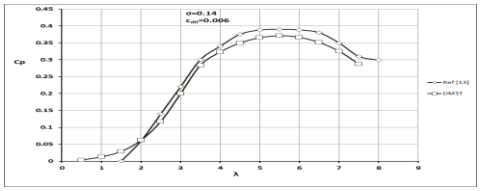

Fig 22: comparison of theoretical results C_p with ref [10] results.

As can be seen from these two figures, a very good agreement exists between the results of the computer program and the results of both references for $\lambda < 5.0$ and a less agreement for $\lambda > 5$.

Conclusions

The following points are considered as a result of this work

1-The comparison of the computer results and with other results [10], [11] indicates that the model used in this study predicts the performance of the rotor fairly well.

2-The starting torque of the rotor increases as the solidity increases; this may help to improve the performance of the vertical axis wind turbines at low tip speed ratios.

3-The power coefficient increases as the rotor blade Reynolds number increases.

4-The results of this study indicate that the self-starting problem of the vertical axis turbine is due to high values of angle of attack at low tip speed ratios, this may help in future in solving this problem. No simple modification to the geometric parameters has much effect on its ability to self-start.

5-These results should also be of value for the structural analysis of such turbines

Future works

The following research points should be considered during the future studies.

- Study the effect of using variable pitch blade and sail blades on the possibility of self-starting of the vertical axis turbine.
- Study the effects of dynamic stall, and shear flow on the performance of the rotor.
- Using Savonius rotor may help to solve the self-starting problem.

References.

[1]. Temple, R. J. "Aerodynamic performance theory for the NRC vertical axis wind turbine", NRC of Canada TRLTR-LA, (1974).

[2]. Jacobs, Eastman N. and Sharman, A. "Airfoil characteristics as affected by variations of the Reynolds number". NACA report No. 586, 1939.

[3]. Critzos, C, C., Heyson, H. H. and Boswinkle, R. W. "Aerodynamic characteristics of NACA 0012 airfoil section at angles of attack from 0 to 180".NACA Tech. Note 3361. 1955

[4]. Sharpe, D. J "Experiments with a Darrieus turbine", Wind power in the United Kingdom symposium, London, July (1978), pp 8-20.

[5]. Healy, J.V "The influence of blade thickness on the out put of vertical axis wind turbines", Wind Engineering, vol. 1, 1978, pp. 1-9.

[6]. Murai, H. , Maruyama, S. and Tsukui, M. "Experimental research on gyromill type vertical axis wind turbine using a sail wing", J. Wind . Eng, vol. 15, (1983), pp. 357-368.

[8]. Robinson, M. L. "The Darrieus wind turbine for electrical power generation", Aeronautical Journal, June. 1981, pp. 244-255.

[9]. Sheldhal, R.E. and Klimas, P.C "Aerodynamic characteristics of seven symmetrical airfoil sections through 180 degrees angle of attack for use in aerodynamic analysis of vertical axis wind turbines", Sandia Laboratories report,
SAND 80-2114, March 1981.

[10] A. Solum, P. Deglaire, S. Eriksson, M. Stålberg, M. Leijon, H. Bernhoff.Design of a 12kW vertical axis wind turbine equipped with a direct driven PM synchronous generator,2006

[11] Paul G.Migliore, John R. Fritschen.Darrieus wind Turbine Airfoil Configurations, June 1982

sjst.scst.edu.ly
Surman Journal for Science and Technology
ISSN: Online (2790-5721) - Print (2790-5713)
مجلة صرمان للعلوم والتقنية
Vol 6, No.2, Jun - Dec. 2024
Pages: 536 - 547

Notation

A	Actuator disc cross sectional area
A_t	Rotor swept area
a	Inflow factor
a_1	Upstream inflow factor
a_2	Downstream inflow factor
C	Blade chord
C_D	Aerofoil sectional drag coefficient
C_{DO}	Aerofoil sectional zero-lift drag coefficient
C_L	Aerofoil sectional lift coefficient
C_N	Aerofoil sectional normal force coefficient
C_T	Aerofoil sectional thrust force coefficient
C_P	Rotor power coefficient (Power/ $(0.5\ V^3\ A_t)$
C_Q	Rotor torque coefficient (Torque/ $(0.5\ V^2\ A_t\ R)$
Cq	Local torque coefficient
D	Rotor drag force
D_S	Savonius rotor diameter
F_X	Average axial blade force
F_{Xb}	Axial blade element force
F_{XL}	Axial stream tube force at first disc
F_{XS}	Axial stream tube force
F_{X1b}	Upstream axial blade force
F_{X1m}	Rate change of momentum through the first disc
F_{X2m}	Rate change of momentum through the second disc
F_{X2b}	Downstream axial blade force
G	Height / diameter ratio
H	Rotor height
$\dot{m}$	Mass flow rate
N	Number of blades
R	Radius of the wind turbine
V_D	Wind velocity through the rotor
V_∞	Free stream velocity
W	Relative resultant velocity
W_1	Local resultant velocity through second disc
W_2	Local resultant velocity through first disc

Greek Notation

Ά	blade angle of attack
α_1	Angle of attack of the first disc
α_2	Angle of attack of the second disc
B	Local azimuth angle
Θ	Blade pitch angle
Λ	Tip speed ratio based on free stream velocity
λ_D	Tip speed ratio based on velocity through the rotor
M	Air viscosity
P	Air density
Σ	Rotor solidity (NC /R)
Ψ	The angle between the resultant velocity vector of Darrieus rotor and the free stream direction